Effects of Frozen Layer on Composite Erosion of Snowmelt and Rainfall in the Typical Black Soil of Northeast China

Qing Bai [1,2]**, Lili Zhou** [2,3]**, Haoming Fan** [2,3]**, Donghao Huang** [2,3,*]**, Defeng Yang** [2,3] **and Hui Liu** [1,2]

1   College of Forestry, Shenyang Agricultural University, Shenyang 110866, China; baiqing0601@126.com (Q.B.); liuhui1994@stu.syau.edu.cn (H.L.)
2   Key Laboratory of Soil Erosion Control and Ecological Restoration in Liaoning Province, Shenyang 110866, China; zhoulilia@163.com (L.Z.); fanhaoming@163.com (H.F.); yangdf@syau.edu.cn (D.Y.)
3   College of Water Conservancy, Shenyang Agricultural University, Shenyang 110866, China
*   Correspondence: donghaohuang@syau.edu.cn

Abstract: Composite erosion caused by snowmelt and rainfall causes considerable soil loss during spring thawing. However, research on the impact of frozen soil layers (FSL) on composite erosion is lacking. Therefore, indoor simulation experiments were conducted on soil conditions of 0 cm (unfrozen soil, FSL_{UN}) and 3 cm thawing depths to explore the influence of FSL on composite erosion in the black soil region of Northeast China. Three snowmelt runoff (SR) discharges ($0.34\ \text{L min}^{-1}$, $0.5\ \text{L min}^{-1}$, and $0.67\ \text{L min}^{-1}$), three rainfall (RF) intensities ($80\ \text{mm h}^{-1}$, $120\ \text{mm h}^{-1}$, and $160\ \text{mm h}^{-1}$), and three snowmelt–rainfall interactions (SRI; $0.34\ \text{L min}^{-1}$–$80\ \text{mm h}^{-1}$, $0.5\ \text{L min}^{-1}$–$120\ \text{mm h}^{-1}$, and $0.67\ \text{L min}^{-1}$–$160\ \text{mm h}^{-1}$) were used in this study. The results indicate that FSL advanced the initial erosion times of SR, RF, and SRI by 42.06%, 43.33%, and 45.83%, respectively. FSL increased the soil erosion rate (SER) of SRI by 1.2 (1.0–1.6) times that of unfrozen soil, which was smaller than that of SR (16.3, 5.6–25.0) and RF (1.7, 1.6–1.9), indicating that the interaction had an inhibitory effect on the increase in water erosion in the frozen layer. Under FSL and FSL_{UN} conditions, RF erosion was 1.5–4.1 times and 14.5–24.3 times greater than SR erosion. The SRI erosion was not a simple linear superposition of multiple types of single-phase erosion; it had a significant nonlinear superposition amplification effect (SAE), with SAE of ~100% and ~300% under frozen and unfrozen soil conditions. Flow velocity ($0.11 < R^2 < 0.68$), stream power ($0.28 < R^2 < 0.88$), and energy consumption ($0.21 < R^2 < 0.87$) exhibited significant ($p < 0.05$) linear relationships with SER in both FSL and FSL_{UN}. The research results deepen our understanding of the composite erosion process during the spring thawing period in the black soil region of Northeast China and provide a basis for the prevention and control of soil erosion in the region.

Keywords: composite erosion; frozen soil layer; snowmelt erosion; rainfall erosion; superposition amplification effect; black soil

1. Introduction

Soil erosion is a major global ecological and environmental concern. Soil erosion damages land resources, reduces soil quality, and seriously endangers agricultural production and grain security [1,2]. Globally, large-scale soil erosion is affected by freeze–thaw processes, especially in high-latitude and high-altitude regions where it is more severe [3]. Water infiltration differs between thawed and subsurface-frozen soils. In contrast to thawed soil, frozen soil has a limited infiltration rate that hinders the downward infiltration of water, forming an interflow in the surface layer of the soil [4]. More than 50% of the soil loss in temperate regions occurs during the thawing period of the frozen soil layer (FSL) [5]. Oygarden [6] conducted a winter rainfall experiment in Norway and found that the main cause of soil loss was the impermeable layer below the surface-thawed soil, namely the FSL, which was the main cause of large-scale and rill erosion. As an impervious layer, the

FSL prevents the infiltration of thawed soil water and limits the infiltration of slope runoff, resulting in an increase in soil water content and a decrease in soil erosion resistance [7]. With an increase in the slope and meltwater flow, the flow velocity of the FSL also increases, and a soil slope with a shallow melting depth produces more sediment than a slope with a deep melting depth [8]. During erosion, there is an interaction between rainfall intensity and melting depth. The initial melting depth is crucial when the rainfall intensity is low. However, it becomes the most dominating factor at high rainfall intensities [9].

Black soil is fertile soil with high organic matter content, clay content, and cementation degree. It is rich in chemical elements such as calcium and magnesium and is widely distributed in Northeast China. The black soil region of Northeast China is an important commodity grain base in the country, with commodity grain supply accounting for one-third of the country. However, due to extensive development and reclamation, black soil has undergone severe degradation, with an average annual decrease in thickness of 0.3–2 mm [10]. The black soil area has a unique erosion environment and belongs to the continental monsoon climate of the cold temperate zone, with obvious seasonal freeze–thaw effects. During the spring thawing period, the FSL begins to thaw from the surface, and the soil is subjected to the effects of "night freezing and day thawing", resulting in increased soil erodibility and increased erosion [11]. Chen et al. [7] studied the water velocities of frozen and unfrozen black soil slopes using the electrolyte tracer method. They obtained flow velocity 30% higher on a 5° frozen slope than on an unfrozen slope. Under low-rainfall-intensity conditions, shallow thawing aggravated the erosion of the partially thawed soil slope. In contrast, under conditions of high rainfall intensity, it is controlled by the soil thawing depth and runoff hydrodynamic conditions [12]. By studying the erosion process under different thawing depths and rainfall intensities and their relationship with hydraulic conditions, it was found that under the same rainfall intensity, the average soil loss rate and range increased with increasing thawing depth [13]. Wang et al. [14] suggested that runoff energy loss could predict the process of soil snowmelt runoff erosion at different thawing depths.

At present, research on the water erosion of FSL during the spring thawing period mainly focuses on the influence of different thawing depths on single-phase water erosion. This was difficult to apply to the interaction between snowmelt runoff (SR) and rainfall (RF). This study used typical black soil to conduct indoor simulation experiments on the composite erosion between the FSL and water erosion forces during the spring thawing period to (1) determine the influence of the FSL on water erosion during the spring thaw and (2) quantify the superposition amplification effect (SAE) of snowmelt–rainfall interaction (SRI) erosion to deepen the understanding of the composite erosion mechanism between the FSL and the water force in the black soil area of Northeast China and provide a scientific basis for erosion control during the spring thawing period.

2. Materials and Methods

2.1. Experimental Material

The experimental soil was obtained from the Jiusan Water Protection Monitoring Station in Nenjiang County, Heilongjiang Province, China. The station is located at 48°59′ N–49°03′ N and 125°16′ E–125°21′ E. The altitude is 310–390 m, the slope is mostly between 3° and 5°, and the length is several hundred to several thousand meters. The climate is a cold temperate continental monsoon climate, the average temperature in January is −22.5 °C, the lowest temperature can reach −43.7 °C, the average annual temperature is 0.4 °C, the average annual effective accumulated temperature is approximately 2100 °C, and the frost–free period is 114 days. The annual average precipitation is 534 mm, mainly from June to August, which accounts for 66.8% of the annual precipitation. The precipitation in spring accounts for 13.1% of the annual precipitation, and there is an average of seven or more strong winds above level 7 during April–May. The soil parent material is Quaternary alluvium and the soil type is black soil, with a PH value of 6.46, which is

slightly acidic, and an organic matter content of 2.49%. The soil texture is classified as silt loam comprised of 9.4% clay, 71.4% silt, and 19.2% sand.

Simulation tests were conducted in an indoor soil composite laboratory at Shenyang Agricultural University. As shown in Figure 1, the experimental devices mainly included a test soil tank (Figure 1a), a freeze–thaw cycle chamber (Figure 1b), an artificially simulated rainfall machine, and a runoff scouring device (Figure 1c). The indoor test soil tank was an impervious steel tank with a size of 1 m (length) × 0.25 m (width) × 0.25 m (depth), and the lower end was connected to a flow collection tank for collecting runoff and sediment samples. The freezing and thawing equipment was AW6000-type low-temperature experimental equipment, mainly composed of a test box, refrigeration unit, electric control box, etc., of which the temperature range was −30–+30 °C and the cooling speed was 3 °C min^{-1} (Shenyang Yileng Refrigerator Co. Ltd., Shenyang, China). The snowmelt runoff water supply device comprised a constant-pressure water tank, a steady flow tank, a water supply tank, a BR-8000 digital speed-regulating peristaltic pump (Niukai Automation Equipment Co. Ltd., Xiamen, China), and a connecting water pipe. The flow range of snowmelt runoff was adjusted to 50–3000 mL min^{-1}, and the steady flow tank was placed on top of the slope of the experimental soil trough and connected to the constant-pressure tank through a connecting water pipe. The experiment used a downpour rainfall simulation system that was divided into three parts: water supply equipment (a water supply tank group and a pressure device), control equipment (an electric control box and a frequency converter), and rainfall equipment(Nanlin Technology Co. Ltd., Nanjing, China). The device was 11 m above the ground, with nozzle diameters of 0.8 mm, 1.5 mm, and 3 mm and a test area of 1.5 m × 1.5 m. There were six rainfall combinations, with a minimum intensity of 30 mm h^{-1} and a maximum intensity of 180 mm h^{-1}. The uniformity of rainfall was 86.5%.
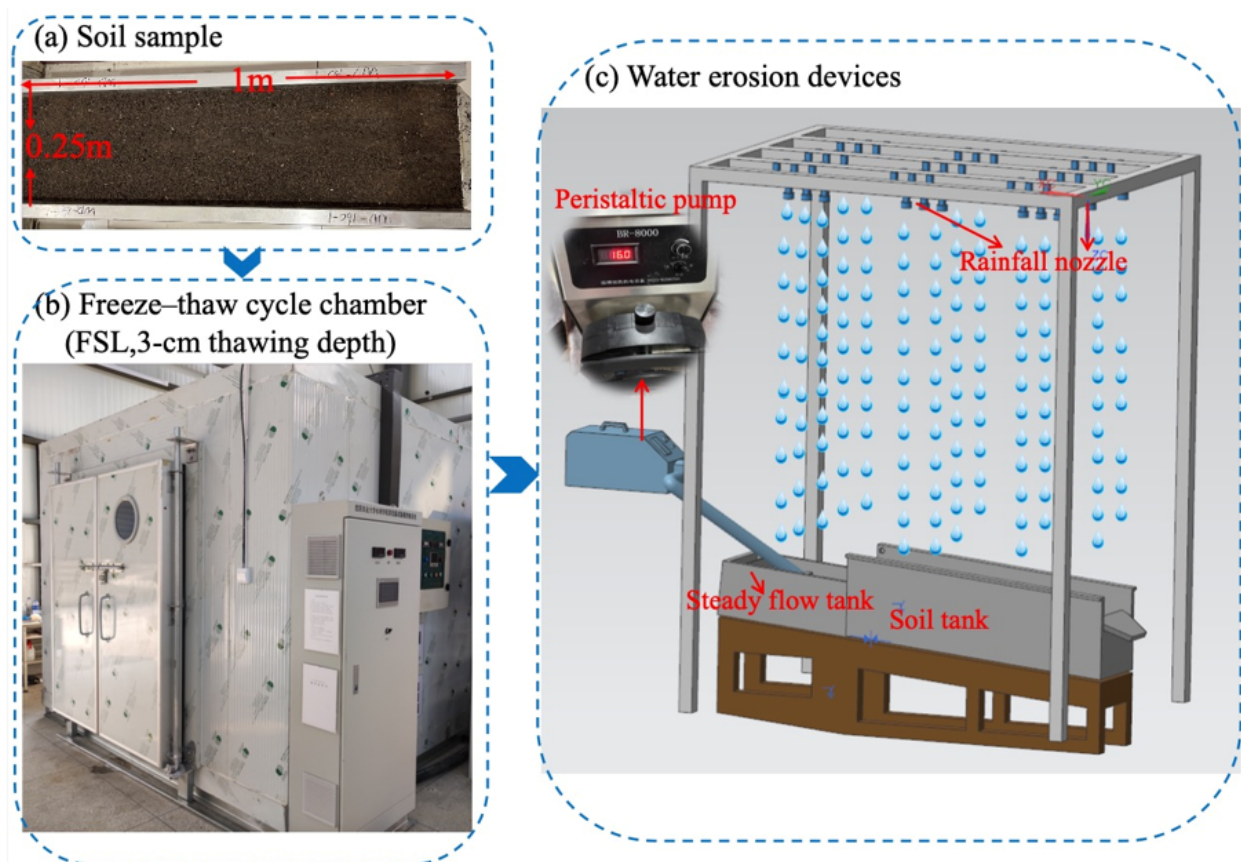

Figure 1. Experimental devices: (**a**) soil sample, (**b**) freeze–thaw devices, and (**c**) water erosion devices.

2.2. Experimental Design

Most landforms in black soil areas have long and gentle slopes, usually between 3° and 7°. The slope of the cultivated land in the experimental soil collection basin was mostly 3°, and based on an investigation by the research group, a slope of 3° in the black soil area can cause serious water erosion. Therefore, this study designed a slope of 3°. The 0–20 cm surface layer of the soil in the research area was the cultivation layer, with a soil bulk density of 1.15 g m^{-3}. Therefore, a filling depth of 20 cm was employed in these experiments. The soil was disturbed for the indoor experiments. The depth of the cultivation layer was 0–20 cm, and the particle size was limited to 1.0 cm after screening. The initial soil water content was set to 1.0 times the field water capacity (~35%), and the soil bulk density was 1.15 g m^{-3}.

Frozen soil layer (FSL) design: According to the field meteorological data of the early spring freeze–thaw period, we set the freezing and melting temperatures at −8 °C and 10 °C, respectively. To ensure that the freezing and melting processes started from the surface of the soil to the bottom, the side and bottom of the soil tank were wrapped with 3 cm thick thermal insulation material. The soil was not completely thawed during the spring thawing period and the surface-thawed soil was easily eroded because of the FSL. Research on the impact of the thawing depth on water erosion has shown that a thawing depth of 5 cm is critical for distinguishing soil erosion under FSL conditions. Starting at 5 cm, the sensitivity of erosion to the thawing depth decreased, and the pattern of change was consistent with that of unfrozen soil slopes [8,15–17]. If the thawing depth is too shallow, the sediment that can be transported is too little, which can easily cause significant experimental errors. Therefore, a thawing depth of 3 cm was used in this study. A soil test tank was placed in a low-temperature environment. After freezing at −8 °C until the soil was completely frozen, it was thawed at 10 °C to a designed depth of 3 cm. The depth of soil thawing was measured using a three-point method with a measuring needle. Then, the soil tank was removed from the low-temperature environment and placed on the experimental steel frame at 3° for the water erosion experiment. The unfrozen soil (FSL$_{UN}$) served as the experimental control.

Water erosion design: The erosive rainfall in the study area is mainly characterized by short-duration and high-intensity rainstorms. In the preliminary experiment, a rainfall intensity of less than 80 mm h^{-1} cannot meet the requirement of producing sediment within 30 min. If the initial sediment production time was extended, it would affect the thawing depth of soil samples. Therefore, we designed three erosive rainfall (RF) intensities: 80, 120, and 160 mm h^{-1}. To ensure comparability with the rainfall experiment, we input the same amount of water during the snowmelt runoff and rainfall experiment (taking the rainfall intensity of 120 mm h^{-1} as an example, it could be converted to 2 mm min^{-1}, so the runoff flow of the rainfall intensity in the 0.25 m^2 soil tank used in the experiment was 0.5 L min^{-1}). Therefore, the snowmelt runoff (SR) flow discharges were 0.34 L min^{-1}, 0.5 L min^{-1}, and 0.67 L min^{-1}. To study the interaction between snowmelt and rainfall water erosion, we designed three snowmelt–rainfall interaction (SRI) conditions: 0.34 L min^{-1}–80 mm h^{-1}, 0.5 L min^{-1}–120 mm h^{-1}, and 0.67 L min^{-1}–160 mm h^{-1}. In other words, the SR and RF experiments were conducted simultaneously. Starting from the input of water on the slope, the test lasted for 20 min with the water temperature of 0 °C–5 °C. Runoff samples were collected every 1 min after sand production was initiated on the slopes, and the sediment mass was weighed at the end of the experiment, dried in a 105 °C oven, and re-weighed (accurate to two decimal places). Each trial was repeated thrice for each of the 54 treatments (Table 1).

Table 1. Experimental design.

Treatment	FSL	FSL$_{UN}$	SR Discharge (L min^{-1})	RF Intensity (mm h^{-1})
FSL–SR$_{0.34}$	$\checkmark$		0.34	
FSL$_{UN}$–SR$_{0.34}$		$\checkmark$	0.34	
FSL–RF$_{80}$	$\checkmark$			80
FSL$_{UN}$–RF$_{80}$		$\checkmark$		80
FSL–SRI$_{0.34–80}$	$\checkmark$		0.34	80
FSL$_{UN}$–SRI$_{0.34–80}$		$\checkmark$	0.34	80
FSL–SR$_{0.5}$	$\checkmark$		0.5	
FSL$_{UN}$–SR$_{0.5}$		$\checkmark$	0.5	
FSL–RF$_{120}$	$\checkmark$			120
FSL$_{UN}$–RF$_{120}$		$\checkmark$		120
FSL–SRI$_{0.5–120}$	$\checkmark$		0.5	120
FSL$_{UN}$–SRI$_{0.5–120}$		$\checkmark$	0.5	120
FSL–SR$_{0.67}$	$\checkmark$		0.67	
FSL$_{UN}$–SR$_{0.67}$		$\checkmark$	0.67	
FSL–RF$_{160}$	$\checkmark$			160
FSL$_{UN}$–RF$_{160}$		$\checkmark$		160
FSL–SRI$_{0.67–160}$	$\checkmark$		0.67	160
FSL$_{UN}$–SRI$_{0.67–160}$		$\checkmark$	0.67	160

Note: $\checkmark$ represents the selected experimental conditions.

2.3. Methods

The soil erosion rate (SER, g m^{-2} min^{-1}) is given by Equation (1):

$$SER = \frac{e_r}{lWt} \tag{1}$$

where e_r is the sediment yield during the observation period (g); l and W are the length and width of the experimental tank, respectively (m); and t is the time (min).

The surface flow velocity (V_s, m s^{-1}) is used to estimate the mean flow velocity (V, m s^{-1}) using Equation (2):

$$V = \beta \cdot V_s \tag{2}$$

where β is a coefficient taken as 0.67 for lamina flow (in this study, Reynolds number (Re) < 500).

The Froude number (Fr) is given by Equation (3):

$$Fr = \frac{V}{\sqrt{g \cdot R}} \tag{3}$$

where g is the gravitational acceleration, m s^{-2}; R is the hydraulic radius, m.

The drag coefficient (f) is given by Equation (4):

$$f = \frac{8gRJ}{V^2} \tag{4}$$

where J is the surface slope and J = sin θ, θ is the slope gradient, °; the meanings of other parameters are the same as before.

The shear stress (τ, Pa) is given by Equation (5):

$$\tau = \rho gRJ \tag{5}$$

where ρ is the volume–weight of flow, kg m^{-3}; the meanings of other parameters are the same as before.

The stream power (w, N m^{-1} s^{-1}) is given by Equation (6):

$$\omega = \tau V \tag{6}$$

where the meanings of other parameters are the same as before.

The calculation of runoff energy consumption (E, J m^{-2} min^{-1}) is given by Equation (7). The process of soil erosion was energy conversion and consumption. According to the law of conservation of energy, the energy of water flowing from any section on the slope was analyzed using the following formula proposed by Li Zhanbin et al. [18]:

$$E_x = q'\rho g(L - x)\sin\theta + \frac{1}{2}q'\rho v_x^2 \tag{7}$$

where q' is the flow rate in the section, J min^{-1}; L is the slope length, x is the distance between any point on slope x and the top of the slope, and v_x is the velocity in section x.

The calculation of the factor contribution rate (P_F, %) is given by Equation (8). The contribution rate of the variance factor of the impact factor to soil erosion was determined using SPSS 19.0 software.

$$P_F = \frac{SS_F - (DOF_F \times V_{Er})}{SS_T} \times 100 \tag{8}$$

where SS_F is the sum of the squares of Type III, DOF_F is the number of degrees of freedom, V_{Er} is the mean square of the error, and SS_T is the total deviation squared.

The superposition amplification effect (SAE %) is given by Equation (9).

$$SAE = \frac{SER_{SRI} - (SER_{SR} + SER_{RF})}{SER_{SR} + SER_{RF}} \times 100 \tag{9}$$

where SER_{SRI} is the SER of SRI, SER_{SR} is the SER of SR, and SER_{RF} is the SER of RF.

3. Results

3.1. Characteristics of SER

The time of initial soil erosion is an important index for evaluating the speed of soil erosion on a slope and reflects the degree of slope erosion. The initial soil erosion time for water erosion is shown in Figure 2. The presence of FSL shortened the initial soil erosion time during water erosion. Specifically, SR, RF, and SRI decreased by 42.1% (0.34 L min^{-1}, 3 min; 0.5 L min^{-1}, 3 min; 0.67 L min^{-1}, 1 min), 43.3% (80 mm h^{-1}, 3 min; 120 mm h^{-1}, 3 min; 160 mm h^{-1}, 2 min), and 45.8% (0.34 L min^{-1}–80 mm h^{-1}, 2 min; 0.5 L min^{-1}–120 mm h^{-1}, 1 min; 0.67 L min^{-1}–160 mm h^{-1}, 0.5 min), respectively. The same amount of water input per unit of time on the frozen surface was compared for the SR and RF erosion. Only 0.34 L min^{-1} SR had a 3 min faster initial soil erosion time than 80 mm h^{-1} RF, and the initial soil erosion times of the other SR and RF erosions were the same, indicating that when the same amount of water was injected per unit time, the water erosion force had little effect on the initial soil erosion time.

The soil erosion rate (SER) is an important parameter for describing the slope erosion process, and its characteristics over time are shown in Figure 3. The SER ranges for different flow discharges of SR with and without FSL were 3.79–13.55 g m^{-2} min^{-1} and 0.24–0.77 g m^{-2} min^{-1}; 5.09–31.61 g m^{-2} min^{-1} and 0.47–3.15 g m^{-2} min^{-1}; and 44.11–61.88 g m^{-2} min^{-1} and 0.83–5.66 g m^{-2} min^{-1} (Figure 3a,d,g). The trend of changes in the SER of SR under the influence of FSL was similar to that of FSL$_{UN}$, and the SER per minute significantly increased during the process. At only 0.34 L min^{-1}, under the influence of the FSL, the peak time of SER advanced by 2 mins, and the active period of SER increased. The effect of the FSL on the active period and the peak time of SER was not significant after the increase in flow discharge. The SER ranges of different intensities of RF erosion with and without FSL were 8.91–15.30 g m^{-2} min^{-1} and

4.92–7.60 g m^{-2} min^{-1}; 11.62–46.63 g m^{-2} min^{-1} and 14.44–30.76 g m^{-2} min^{-1}; and 57.39–130.42 g m^{-2} min^{-1} and 34.98–72.88 g m^{-2} min^{-1} (Figure 3b,e,h). RF erosion under the influence of the FSL significantly increased the fluctuation of the erosion process and the value of SER per minute influenced the occurrence time of erosion peaks (FSL–RF$_{80}$, 8 min; FSL–RF$_{120}$, 6 min; and FSL–RF$_{160}$, 3 min). The SER ranges of different intensities of SRI erosion with and without FSL were 33.83–45.68 g m^{-2} min^{-1} and 26.81–54.60 g m^{-2} min^{-1}; 102.60–166.65 g m^{-2} min^{-1} and 43.53–106.28 g m^{-2} min^{-1}; and 107.69–161.71 g m^{-2} min^{-1} and 77.71–190.49 g m^{-2} min^{-1} (Figure 3c,f,i). The fluctuation in the SRI erosion process was reduced by the FSL, and except for the combination of minimum discharge and intensity, it showed a trend of first increasing and then decreasing and tended to stabilize, with the peak appearing within five minutes after the occurrence of erosion. This is evidence of the hysteresis effect. When RF and SR erosion input the same amount of water per unit of time, the peak time of the former (2–17 min) was earlier than that of the latter (8–20 min), and the average SER was higher, indicating that raindrop splashing accelerated the erosion resistance of the soil. The trend of the soil erosion process in the SRI erosion was more similar to that in the RF erosion under the same conditions. In most cases, the erosion peak and inflexion points occurred at the beginning of water erosion and less than 10 min after soil erosion.
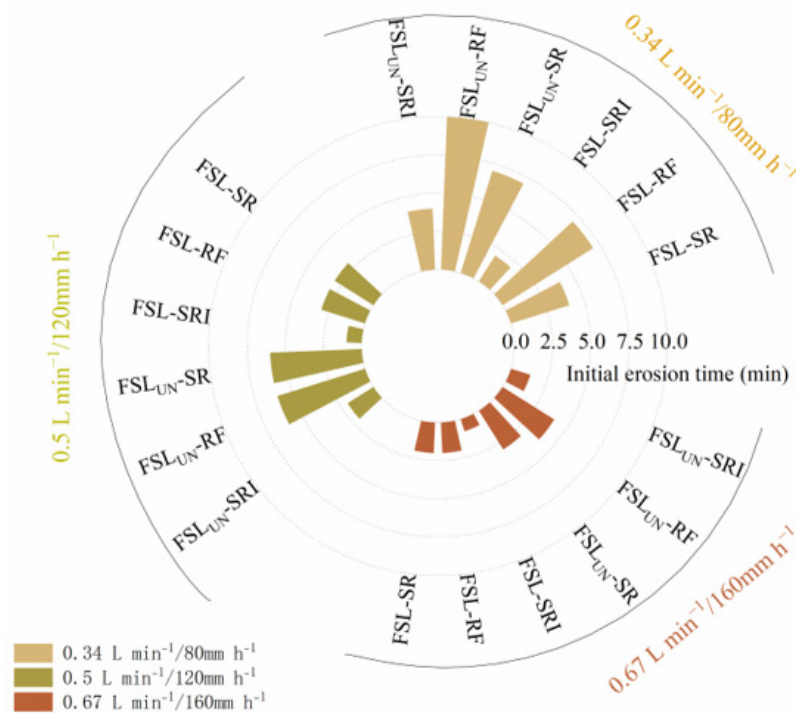

Figure 2. Time of initial soil erosion, where numbers represent discharge and intensity.

Figure 4 shows the effects of the FSL on the SER under different water erosion forces. It can be observed from the figure that under the same combination of discharge and intensity, the SER of SR erosion was the most concentrated, followed by that of RF. The most unstable date was that of the SRI erosion, and this phenomenon was more evident in FSL$_{UN}$. FSL increased the SER by 16.33 (SR$_{0.34}$ = 7.87 g m^{-2} min^{-1}; SR$_{0.5}$ = 8.54 g m^{-2} min^{-1}; SR$_{0.67}$ = 53.38 g m^{-2} min^{-1}), 1.70 (RF$_{80}$ = 12.03 g m^{-2} min^{-1}; RF$_{120}$ = 35.41 g m^{-2} min^{-1}; RF$_{160}$ = 83.91 g m^{-2} min^{-1}), and 1.22 (SRI$_{0.34–80}$ = 40.55 g m^{-2} min^{-1}; SRI$_{0.5–120}$ = 130.48 g m^{-2} min^{-1}; SRI$_{0.67–160}$ = 134.06 g m^{-2} min^{-1}) times that of FSL$_{UN}$. Among these, FSL had the greatest and least impacts on SR and SRI, respectively. Because the FSL hindered infiltration, SR was equivalent to increasing runoff; therefore, the impact was the greatest. Raindrops and runoff had an inhibitory effect; therefore, their impact on erosion with rainfall was relatively small. Regardless of the influence of the FSL,

the average SER from RF erosion was higher than that from SR erosion for the same amount of water input per unit of time. Under FSL and FSL_{UN} conditions, RF erosion was 1.53–4.14 times and 14.53–24.27 times greater than that of SR erosion, respectively. The linear accumulation of the erosional forces of SR and RF was compared with that of SRI erosion. When FSL was present, the SRI erosion had a significant nonlinear SAE of 99.43% (0.34 L min^{-1}/80 mm h^{-1}:103.71%; 0.5 L min^{-1}/120 mm h^{-1}:196.86%; 0.67 L min^{-1}/160 mm h^{-1}: −2.35%). In the FSL_{UN}, the SAE reached 296.40% (0.34 L min^{-1}/80 mm h^{-1}:515.94%; 0.5 L min^{-1}/120 mm h^{-1}:249.15%; 0.67 L min^{-1}/160 mm h^{-1}:124.43%), and as the discharge/intensity increased, the SAE weakened. SRI erosion was not a simple linear superposition of multiple types of single-phase water erosion but had a significant nonlinear SAE. The FSL reduced the SAE because the SER of the SRI was greater than the thawing rate of the FSL, and the unthawed soil below the FSL failed to meet the erosion needs promptly. Regardless of the influence of FSL, the median SER of RF erosion was always greater than that of SR erosion, and the sum of the two was always smaller than that of SRI water erosion. The chart shows individual anomalous values owing to the hysteresis effect of sediments, which suddenly scoured the trough when they were moved to the bottom of the soil by runoff transport, resulting in an abnormal increase in erosion.
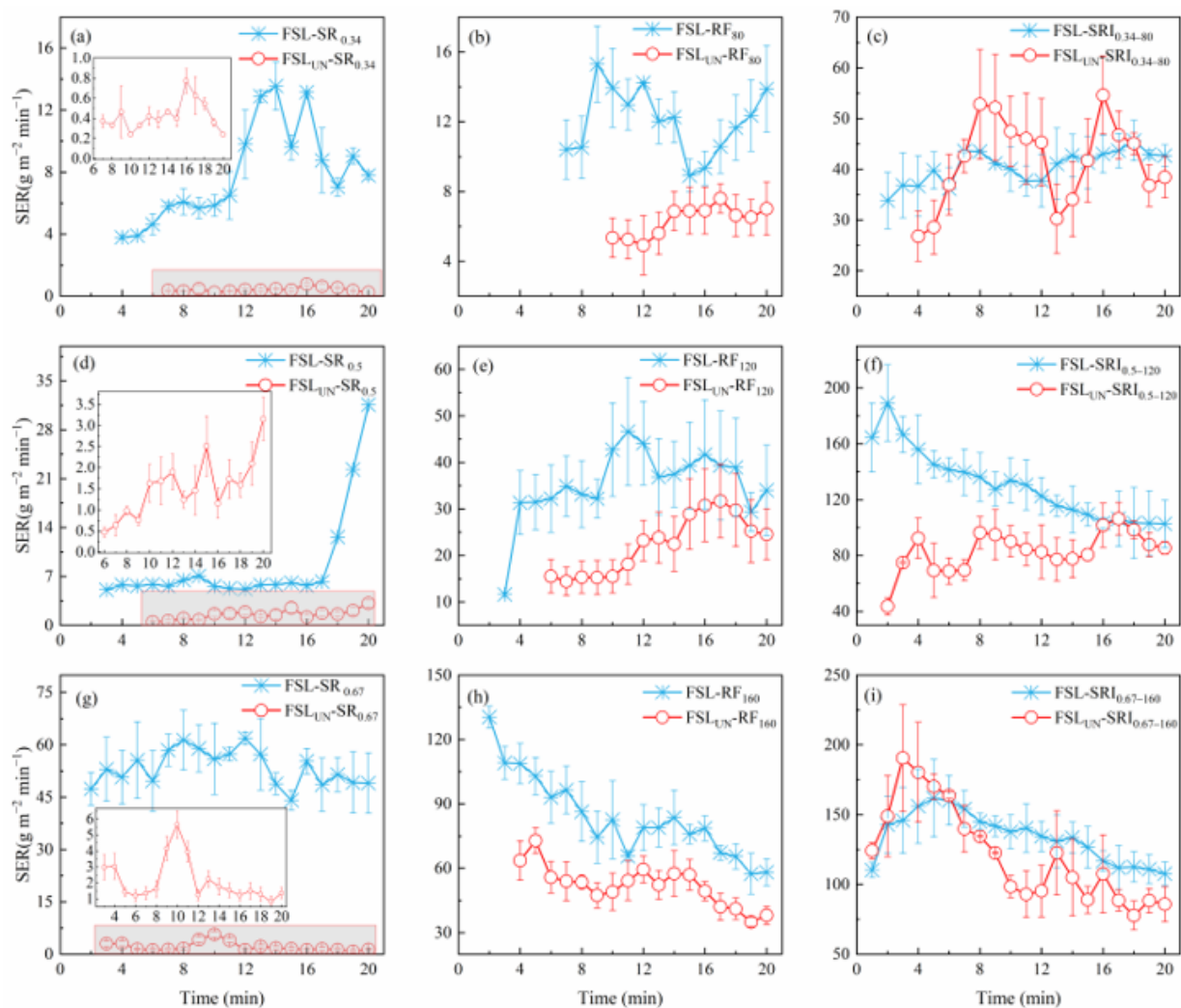

Figure 3. Characteristics of soil erosion over time. And, (**a**) for $SR_{0.34}$; (**b**) for RF_{80}; (**c**) for $SRI_{0.34-80}$; (**d**) for $SR_{0.5}$; (**e**) for RF_{120}; (**f**) for $SRI_{0.5-120}$; (**g**) for $SR_{0.67}$; (**h**) for RF_{160}; (**i**) for $SRI_{0.67-160}$.
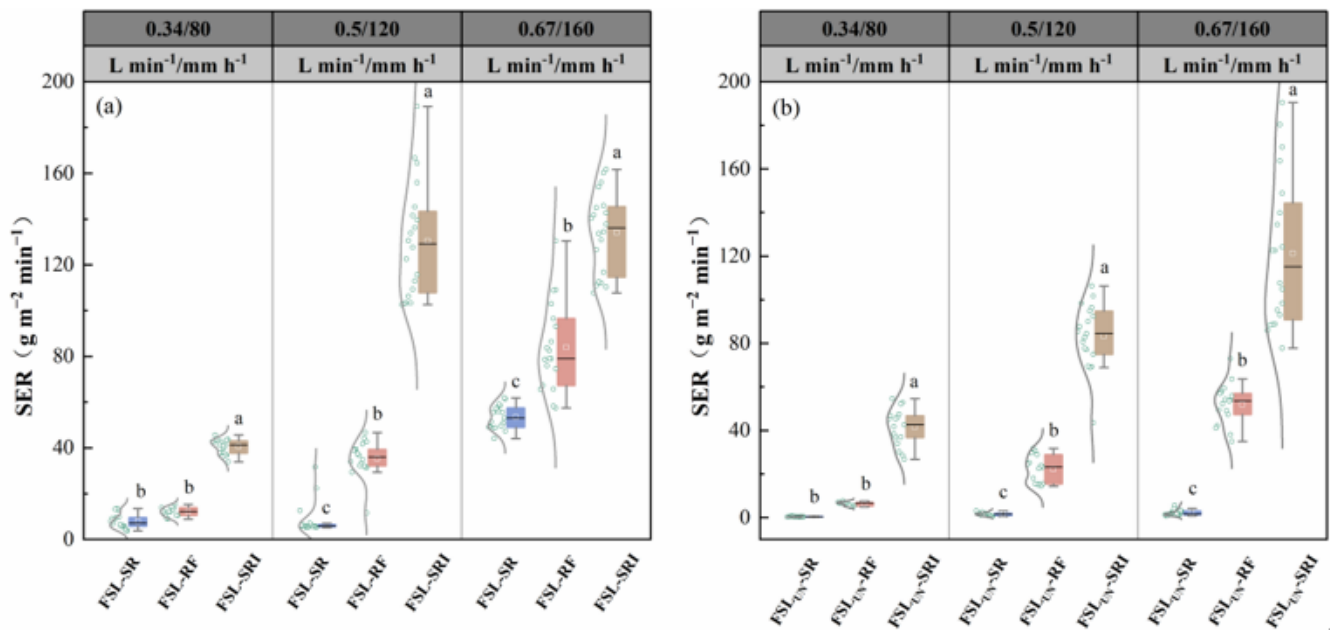
Figure 4. Soil erosion rate under different water erosion forces: (**a**) Under FSL conditions, (**b**) Under FSL$_{UN}$ conditions. Different lowercase letters indicate the differences in SER between water erosion forces (Person, $p < 0.05$).

3.2. Hydraulic Parameters Affecting Soil Erosion

Figure 5 shows the contribution of the FSL to the water erosion hydraulic parameters under different water forces. The FSL plays an active role in determining the mean flow velocity and Froude number during water erosion. Specifically, the FSL increased the average flow velocity of the water erosion, in which SR increased by 14.39%, RF increased by 4.77%, and SRI by 8.83%. In addition, the FSL also increased the Froude number, in which SR increased by 15.04%, RF increased significantly by 123.59%, and SRI increased by 27.99%. It is worth noting that only when there was an intensity of 160 mm h^{-1} in the FSL did the RF cause torrent erosion; in other cases, it caused slow flow erosion. Therefore, the results highlight the important contribution of the FSL in this respect. However, the FSL reduces the drag coefficient and energy consumption. Specifically, the SR drag coefficients decreased by 20.85%, the RF drag coefficient decreased by 55.39%, and the SRI drag coefficient decreased by 42.85%. The SR energy consumption decreased by 12.12%, RF energy consumption decreased by 1.31%, and SRI energy consumption decreased by 0.11%; this indicated that an impervious surface layer can effectively alleviate RF drag and consume less energy. The flow of SR occurred as sheet flow, while the flow for RF was channelized. The contributions of the FSL to other hydraulic parameters showed different trends under the influence of the water erosion force, and the responses of the SR, average flow width of the rainfall force, shear stress, and stream power to the FSL showed opposite trends. For example, the FSL contributed negatively to the flow width of SR and positively to RF erosion. The variation law of the hydraulic parameters of the SRI erosion was similar to that of the RF erosion, which could explain why the influence of the FSL on the SER of the SRI erosion obtained in Section 3.1 was more similar to that of the RF erosion. By comprehensively considering the influence of the presence of the FSL on the SER of various water erosion forces in Section 3.1, it can be concluded that the FSL mainly increased the SER by reducing the average energy consumption.
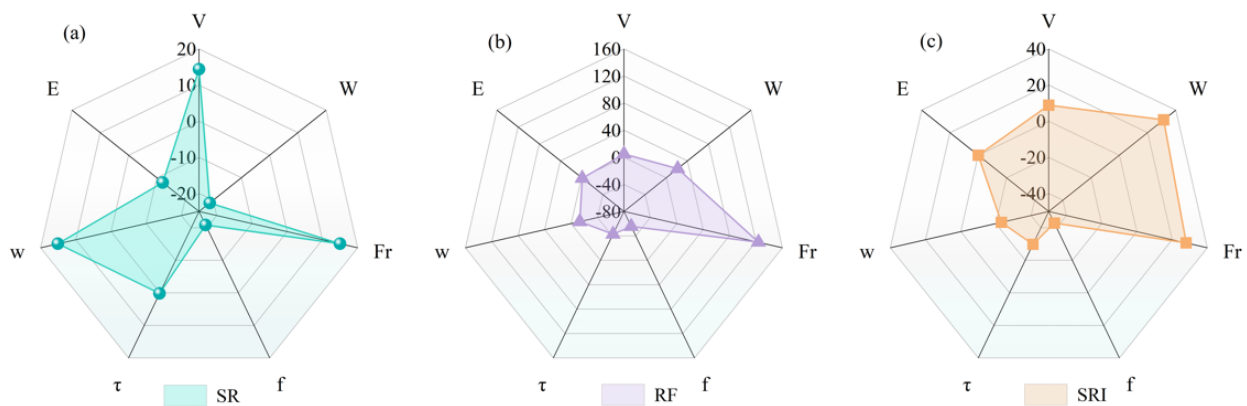
Figure 5. Contribution rate of FSL to hydraulic parameters of different water erosion forces (%): (**a**) snowmelt runoff; (**b**) rainfall; (**c**) the interaction of snowmelt–rainfall. V represents flow velocity; W represents the flow width; Fr represents the Froude number; f represents the drag coefficient; τ represents the shear stress; w represents the stream power; and E represents the energy consumption.

Figure 6 shows the characteristics of the various hydraulic parameters under different water erosion forces. The SR had a faster average flow velocity, larger stream power, and a larger Froude number than the RF. Specifically, the average flow velocity of SR (0.14 m s^{-1}, 0.12 m s^{-1}) was 3.5 and 3.0 times the RF (0.04 m s^{-1}, 0.04 m s^{-1}) erosion when FSL and FSL_{UN}, respectively. The average stream power of SR ($0.07 \text{ N m}^{-1} \text{ s}^{-1}$, $0.06 \text{ N m}^{-1} \text{ s}^{-1}$) was 1.4 and 1.04 times the RF ($0.05 \text{ N m}^{-1} \text{ s}^{-1}$, $0.06 \text{ N m}^{-1} \text{ s}^{-1}$) erosion, respectively. In addition, SR presented a sharp pattern compared with RF erosion, whereas RF invasion presented a slow pattern. However, compared to RF erosion, the average flow width, drag coefficient, shear stress, and energy consumption of SR were smaller. Specifically, the flow width of SR (0.54 dm, 0.69 dm) was 0.63 and 0.97 times the RF (0.86 dm, 0.71 dm) erosion for FSL and FSL_{UN}, respectively. The drag coefficient along the slope flow of SR (0.21, 0.27) was 0.08 and 0.04 times the RF erosion (2.74, 6.13), respectively. The shear stress generated along the flow direction of SR (0.48 Pa, 0.48 Pa) was 0.63 and 0.36 times the RF erosion (0.76 Pa, 1.34 Pa), respectively. The energy consumption of SR ($0.21 \text{ J m}^{-2} \text{ min}^{-1}$, $0.24 \text{ J m}^{-2} \text{ min}^{-1}$) was 0.88 and 0.96 times the RF erosion ($0.24 \text{ J m}^{-2} \text{ min}^{-1}$, $0.25 \text{ J m}^{-2} \text{ min}^{-1}$), respectively. In other words, RF erosion can separate and transport sediments by increasing the flow width, drag coefficient, and shear stress and generating higher energy consumption, resulting in a higher SER than SR. For SRI erosion, there was an interaction between the SR and RF. When the hydraulic parameter value of the SRI erosion was between those of the SR and RF, the two forces had opposite effects on the hydraulic characteristics. When the hydraulic parameter value of composite water erosion was higher than the single operating force value, the two operating forces promoted each other's hydraulic characteristics. As shown in Figure 6, in the process of SRI erosion, the values of the flow velocity, Froude number, and drag coefficient were between the values of SR or RF erosion only; that is, $V_S > V_{S-R} > V_R$, $Fr_S > Fr_{S-R} > Fr_R$, and $f_R > f_{S-R} > f_S$, which shows that the introduction of the RF force can inhibit the flow velocity and Froude number of the simple runoff force. Runoff can also reduce the drag resistance to rainfall erosion. However, the addition of another agent to the SRI erosion promoted the flow width, shear stress, stream power, and energy consumption of single water erosion. Among them, the energy consumed by the SRI erosion was higher than the sum of the cumulative single-phase water erosion, which also explains why the average SER of the SRI erosion in Section 3.1 was higher than the sum of the average SER of a single water erosion operating force in most cases.
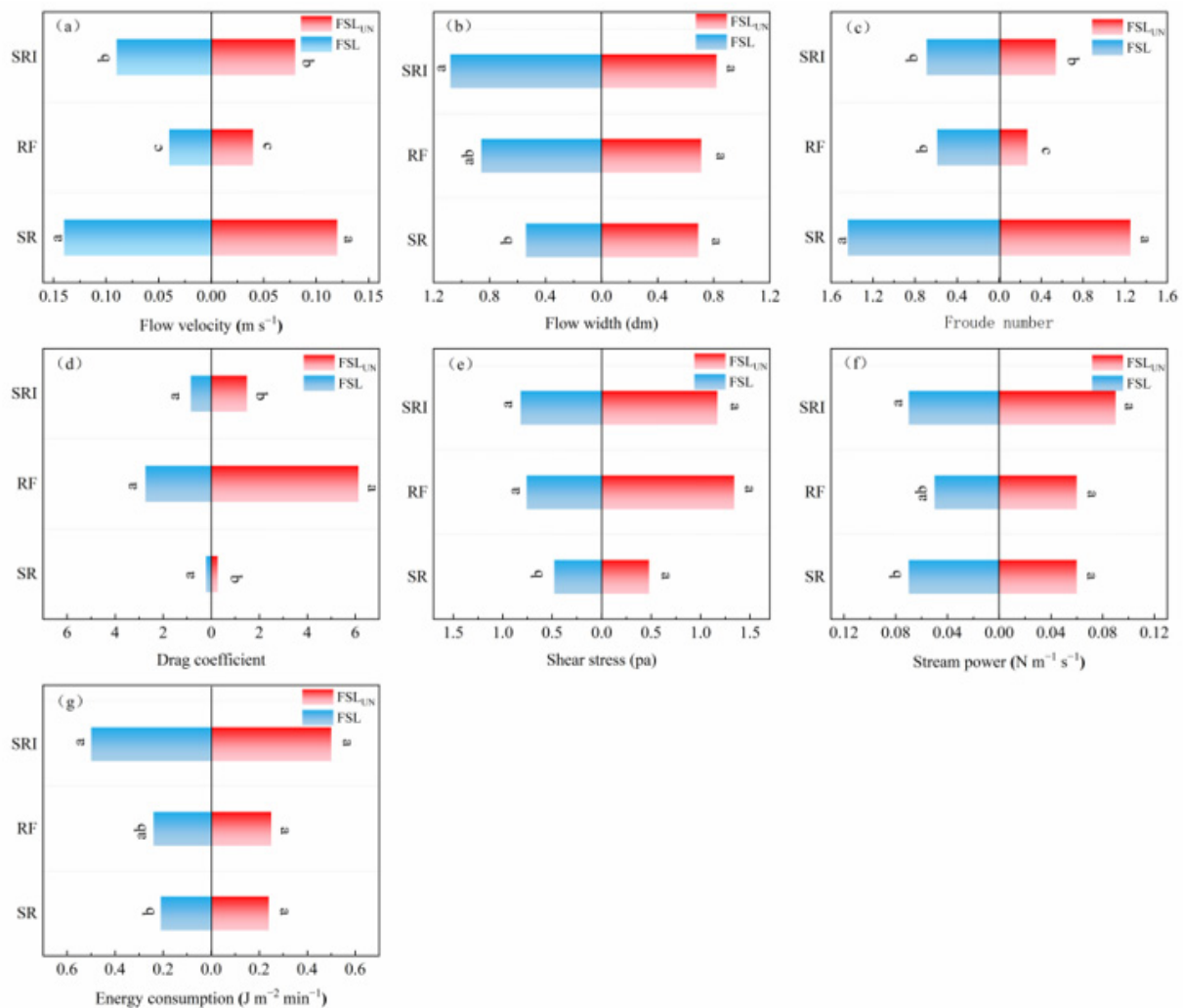
Figure 6. Values of hydraulic parameters of different water erosion forces under FSL and FSL$_{UN}$ conditions: (**a**) flow velocity; (**b**) flow width; (**c**) Froude number; (**d**) drag coefficient; (**e**) shear stress; (**f**) stream power; (**g**) energy consumption. Different lowercase letters indicate the differences in hydraulic parameter values between water erosion forces (Person, *p* < 0.05).

The hydraulic parameters corresponding to the maximum correlation coefficient under different working conditions were selected through the linear fitting of the SER and various hydraulic parameters. Finally, the three hydraulic parameters of flow velocity (0.11 < R^2 < 0.68), stream power (0.28 < R^2 < 0.88), and energy consumption (0.21 < R^2 < 0.87) fit well with the SER. Therefore, in this study, we analyzed three hydraulic parameters. The regression equations between the SER and the flow velocity, stream power, and energy consumption of different water erosion forces under FSL and FSL$_{UN}$ are shown in Figure 7. Soil erosion occurs only when the hydraulic parameters of slope runoff exceed critical values. The critical flow velocities of SR in FSL and FSL$_{UN}$ were 0.11 m s^{-1} and 0.08 m s^{-1} (Figure 7a), respectively, and those of RF was 0.04 m s^{-1} and 0.03 m s^{-1} (Figure 7d). The critical flow velocity caused by SRI was 0.07 m s^{-1} and 0.06 m s^{-1} (Figure 7g). In addition, the critical stream powers of SR water erosion in FSL and FSL$_{UN}$ were 0.033 N m^{-1} s^{-1} and 0.026 N m^{-1} s^{-1} (Figure 7b), respectively, and those of RF water erosion were 0.018 N m^{-1} s^{-1} and 0.028 N m^{-1} s^{-1} (Figure 7e), respectively. The critical stream power of SRI was 0.039 N m^{-1} s^{-1} and 0.022 N m^{-1} s^{-1} (Figure 7h), respectively. The critical energy consumption of SR erosion in FSL and FSL$_{UN}$ was 0.133 J m^{-2} min^{-1} and 0.114 J m^{-2} min^{-1} (Figure 7c), and the critical energy consumption of RF erosion was 0.151 J m^{-2} min^{-1} and 0.152 J m^{-2} min^{-1} (Figure 7f), respectively. The critical energy

consumption of SRI erosion was 0.131 J m^{-2} min^{-1} and 0.154 J m^{-2} min^{-1} (Figure 7i). Considering the influence of the FSL on the SER, the variation in the critical flow velocity is consistent with the above results. In other words, the FSL increased the critical flow velocity of water erosion. Specifically, the SR increased the critical flow velocity by 0.03 m s^{-1}. The RF increased the critical flow velocity by 0.01 m s^{-1}. For the SRI, the critical flow velocity increased by 0.01 m s^{-1}. Before the soil particles separated and moved, only the accumulated water velocity exceeded the critical value, causing soil particle erosion. Because the soil above the FSL is destroyed by freeze–thaw cycles and forms a large amount of sediment, a higher critical flow velocity is required for its separation and transport. Under the same water input, SR and RF erosion had different characteristics. RF enhanced the soil erosion capacity by increasing critical energy consumption.
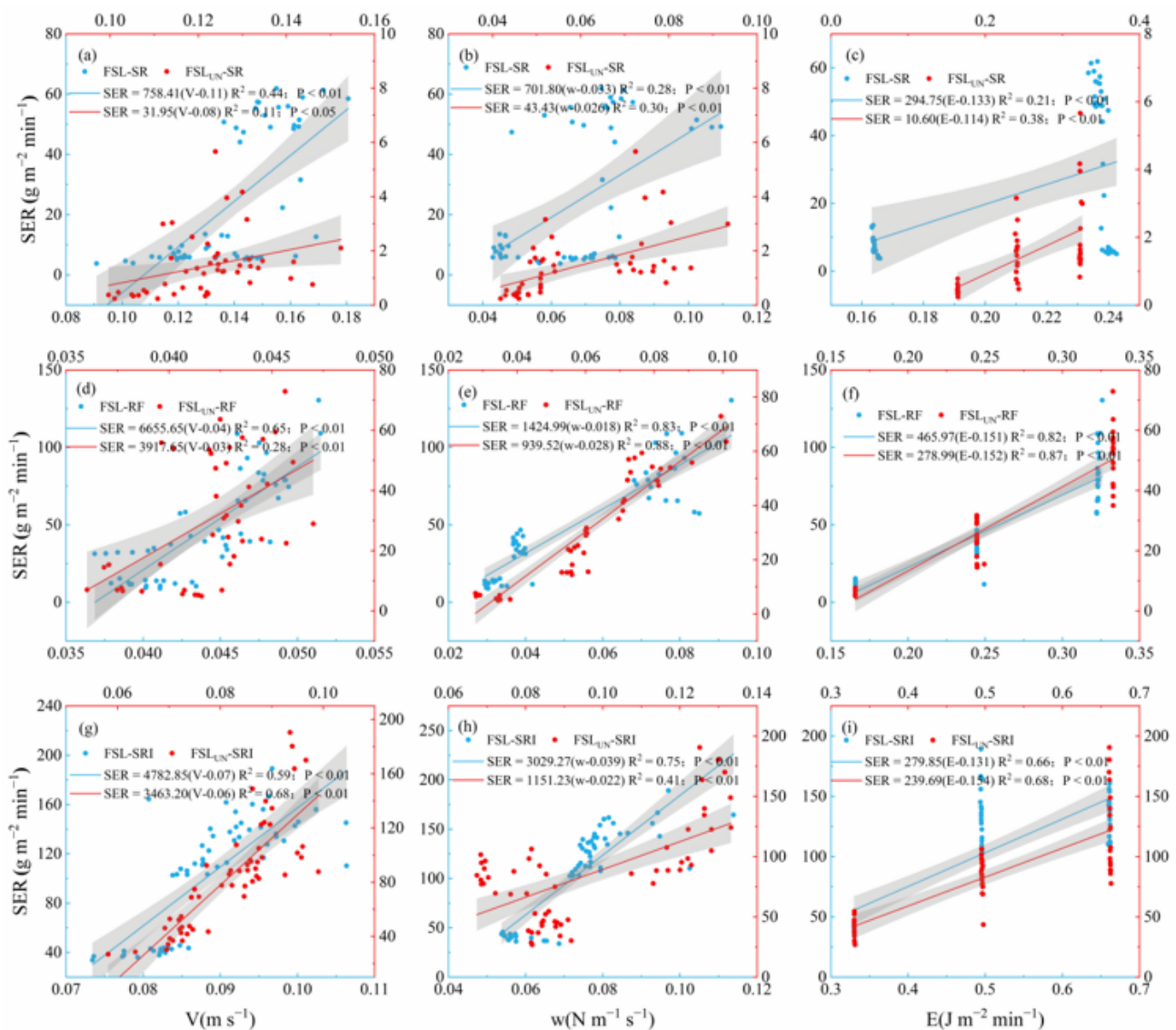

Figure 7. Regression equations between SER and V, w, and E of different water erosion forces under FSL and FSL$_{UN}$, where V represents flow velocity, w represents stream power, and E represents energy consumption. (**a**) Regression equations between SER and V of SR; (**b**) Regression equations between SER and w of SR; (**c**) Regression equations between SER and E of SR; (**d**) Regression equations between SER and V of RF; (**e**) Regression equations between SER and w of RF; (**f**) Regression equations between SER and E of RF; (**g**) Regression equations between SER and V of SRI; (**h**) Regression equations between SER and w of SRI; (**i**) Regression equations between SER and E of SRI.

4. Discussion

Water erosion is easily affected by FSL covered with thawed topsoil [19]. This is because the FSL forms a highly impermeable layer, which prevents the normal infiltration of runoff and intensifies the surface runoff, making it easier to concentrate. Soil erosion is also positively correlated with surface runoff [20]. Additionally, the physical and chemical properties, structure, and texture of the soil in the upper part of the frozen layer change under freeze–thaw action, exacerbating erosion [15,21–23]. The FSL intensifies water erosion, as shown in Table 2. The erosion range of the FSL on the RF is the same as that used in this study. The reason for the difference in runoff erosion is mainly the thawing depth, and the effect of FSL is not significant when greater than 5 cm [24]. In this study, the FSL increased the flow velocity and Froude number and reduced the drag coefficient and energy consumption. This is consistent with the fact that there is a lower drag and faster water flow velocity under FSL conditions [8,24,25].

Table 2. The impact of FSL on erosion.

Author	Soil Type	Slope Gradient	Force	Discharge/Intensity	Thawing Depth (cm)	Increased Erosion
Wang (2021) [26]	Black soil	5°	runoff	1 L min^{-1}, 4 L min^{-1}	5, 10	10–13.5%, 15.4–37.1%
Wang (2020) [13]	Loessial soil	15°	rainfall	0.6 mm min^{-1}, 0.9 mm min^{-1}, 1.2 mm min^{-1}	2, 4, 6	41.1–122.7%, 45.5–315.1%, 83.4–430.1%
Sharratt (2000) [15]	Hattie clay, Barnes loam	7%	rainfall	96 mm h^{-1}	1, 2, 5	100%, 50%

In this study, soil erosion due to RF erosion under the same water input conditions per unit time was higher than that due to SR erosion, and rainfall was one of the main influencing factors. Li et al. [27] compared the slope erosion of typical black soil with and without RF energy and found that RF energy significantly increased the amount of erosion, which is consistent with the results of this study. According to the statistics, raindrop erosion accounts for 72.3–96.2% of the total soil erosion. Eliminating the influence of raindrops significantly reduces runoff and sediment concentrations. From the perspective of water hydraulic characteristics, after excluding the influence of raindrops, the flow depth, flow velocity, Reynolds number, and Froude number decreased from 3.85% to 39.34%, 20.9% to 67.5%, 25.82% to 70.29%, and 18.75% to 62.50%, respectively. The velocity is a key hydraulic parameter that plays an important role in raindrop erosion. Compared with the raindrop-free impact treatment, the critical shear stress, critical unit stream power, and critical stream power increased by more than two times after raindrop impact [28]. In this study, the influence of RF erosion led to a widening of the erosion width, an increase in erosion sources, and an increase in shear stress and energy consumption, which resulted in a higher SER than SR with the same input water quantity [29]. This was because the same amount of water was input into the test soil tank, but the splashing effect of raindrops increased the ability of the water flow to peel off the slope surface, increasing the sand content. Sediment erosion increased resulting in a greater sediment yield. Therefore, the required critical energy consumption increases correspondingly. RF erosion can be fitted using stream power, whereas runoff erosion can be fitted using energy consumption [30,31]. However, unlike some studies, we did not find that shear stress can effectively describe the sediment changes [3,13,26]. As shown in Table 3, the main reason for the different fitting results was that the soil erosion and hydraulic parameters varied with soil type, slope gradient, and flow discharge.

Table 3. Fitting equations for SER and hydraulic parameters.

Author	Soil Type	Slope Gradient (°)	Force	Discharge/Intensity	Equation
An (2012) [28]	Loessial soil	5, 7.5, 10	rainfall	50, 75, 100 mm h^{-1}	SER = 0.43w − 0.0395
Li (2016) [32]	Black soil	5, 10	runoff–rainfall	50 mm h^{-1}, 50–300 L min^{-1}	SER = 0.047(w − 0.611)
Wang (2020) [13]	Loessial soil	15	rainfall	0.6, 0.9, 1.2 mm min^{-1}	SER = 784.18w$^{0.61}$
Wang (2020) [14]	Loessial soil	15	runoff	1, 2, 4 L min^{-1}	SER = 2.65 × ln(E − 4.01)

Note: where SER is the soil erosion rate, g m^{-2} min^{-1}, w is the stream power, N m^{-1} s^{-1}, and E is the energy consumption, J m^{-2} min^{-1}.

The synergistic effects of the upslope inflow and rainfall on the slope would intensify soil erosion. Compared to the pure runoff treatment, soil erosion increased by 1.4–14 times [31]. Composite erosion was not a linear superposition of multiple types of single-phase erosion but a significant nonlinear superposition amplification effect [33]. Li et al. [32] studied the effects of incoming water on downslope erosion, the results showed that with upslope inflow, soil loss increases by 12 to 1950 times compared to without upslope inflow. The results of this study show that the SRI leads to a greater SER than the linear superposition of a single-phase water erosion, which is consistent with the results of previous studies. In the absence of FSL effects, RF plays a dominant role in increasing interlayer erosion during SRI erosion [34]. The contributions of the SR and RF factors to the SRI are shown in Table 4, and the RF factors also play a dominant role.

Table 4. Contribution of SR and RF factors in SRI erosion.

Factor	FSL		FSL$_{UN}$	
	P$_F$ (%)	*p*-Values	P$_F$ (%)	*p*-Values
SR	12.58	<0.01	17.56	<0.01
RF	25.77	<0.01	45.55	<0.01

Overall, the results of this study differ from those of other studies because of the different soil types, slope gradients, and flow discharges. This study provides basic data for the study of springwater erosion in the black soil region of Northeast China. In future research, the erosion in different regions and seasons should be fully considered. It is important to quantify erosion differences and distinguish the main control factors.

5. Conclusions

This study involved experimental research on the erosion process of black soil slopes under the influence of FSL and water erosion forces. The results show that the FSL advanced the initial erosion time and increased the SER and that the interaction had an inhibitory effect on the increase in water erosion in the frozen layer. RF erosion under the influence of raindrops was more severe than SR erosion with the same amount of input water. SRI erosion is not a simple linear superposition of multiple types of single-phase erosion but has a significant nonlinear SAE. RF was the dominant driving force for SRI erosion. Flow velocity ($0.11 < R^2 < 0.68$), stream power ($0.28 < R^2 < 0.88$), and energy consumption ($0.21 < R^2 < 0.87$) exhibited significant ($p < 0.05$) linear relationships with SER in both FSL and FSL$_{UN}$. These findings can help distinguish the key influencing factors in composite erosion to develop more effective prevention and control measures. There are differences in the ways in which seasonal freeze–thaw affects water erosion. Therefore, the impacts of freeze–thaw on water erosion and its hydrodynamic mechanism under different superposition methods are worth further research.

References

1. Sartori, M.; Ferrari, E.; M'Barek, R.; Philippidis, G.; Boysen-Urban, K.; Borrelli, P.; Montanarella, L.; Panagos, P. Remaining loyal to our soil: A prospective integrated assessment of soil erosion on global food security. *Ecol. Econ.* **2024**, *219*, 108103. [CrossRef]
2. Ayoubi, S.; Rabiee, S.; Mosaddeghi, M.; Abdi, M.; Abbaszadeh, F. Soil erosion and properties as affected by fire and time after fire events in steep rangelands using 137 Cs technique. *Arab. J. Geosci.* **2021**, *14*, 113. [CrossRef]
3. Zhang, K.; Bai, Y.; Wang, X.; Xu, X. Modeling the sediment transport capacity on non–erodible frozen soil slope of overland flow. *Catena* **2022**, *212*, 106102. [CrossRef]
4. Wu, Z.; Fang, H. Snowmelt erosion: A review. *Earth-Sci. Rev.* **2024**, *250*, 104704. [CrossRef]
5. Froese, J.C.; Cruse, R.M.; Ghaffarzadeh, M. Erosion mechanics of soils with an impermeable subsurface layer. *Soil Sci. Soc. Am. J.* **1999**, *63*, 1836–1841. [CrossRef]
6. Oygarden, L. Rill and gully development during an extreme winter runoff event in Norway. *Catena* **2003**, *50*, 217–242. [CrossRef]
7. Chen, C.; Ban, Y.; Lei, T.; Feng, R.; Gao, Y. Water flow velocity over frozen and nonfrozen black soil slopes. *Hydrol. Process.* **2018**, *32*, 2231–2238. [CrossRef]
8. Ban, Y.; Lei, T.; Chen, C.; Yin, Z.; Qian, D.F. Meltwater erosion process of frozen soil as affected by thawed depth under concentrated flow in high altitude and cold regions. *Earth Surf. Proc. Land.* **2017**, *42*, 2139–2146. [CrossRef]
9. Su, Y.; Zhang, Y.; Wang, H.; Lei, N.; Li, P.; Wang, J. Interactive effects of rainfall intensity and initial thaw depth on slope erosion. *Sustainability* **2022**, *14*, 3172. [CrossRef]
10. Zheng, F.; Zhang, J.; Liu, G.; Fan, H.; Wang, B.; Shen, H. Characteristics of soil erosion on sloping farmlands and key fields for studying compound soil erosion caused by multi-forces in Mollisol region of Northeast China. *Bull. Soil Water Conserv.* **2019**, *39*, 314–319. [CrossRef]
11. Sun, B.; Xiao, J.; Li, Z.; Ma, B.; Zhang, L.; Huang, Y.; Bai, L. An analysis of soil detachment capacity under freeze-thaw conditions using the Taguchi method. *Catena* **2018**, *162*, 100–107. [CrossRef]
12. Gao, X.; Shi, X.; Lei, T. Influence of thawed soil depth on rainfall erosion of frozen bare meadow soil in the Qinghai–Tibet Plateau. *Earth Surf. Proc. Land.* **2021**, *46*, 1953–1963. [CrossRef]
13. Wang, W.; Li, Z.; Yang, R.; Wang, T.; Li, P. Experimental study of freeze–thaw/water compound erosion and hydraulic conditions as affected by thawed depth on loessal slope. *Front. Environ. Sci.* **2020**, *8*, 609594. [CrossRef]
14. Wang, T.; Li, P.; Liu, Y.; Hou, J.; Li, Z.; Ren, Z.; Hinkelmann, R. Experimental investigation of freeze–thaw meltwater compound erosion and runoff energy consumption on loessal slopes. *Catena* **2020**, *185*, 104310. [CrossRef]
15. Sharratt, B.S.; Lindstrom, M.J.; Benoit, G.R.; Young, R.A.; Wilts, A. Runoff and soil erosion during spring thaw in the northern US Corn Belt. *J. Soil Water Conserv.* **2000**, *55*, 487–494.
16. Gao, X.; Li, F.; Chen, C.; Ban, Y.; Gao, Y. Effects of thawed depth on the sediment transport capacity by melt water on partially thawed black soil slope. *Land Degrad. Dev.* **2019**, *30*, 84–93. [CrossRef]
17. Chen, C. *Erosion Mechanism and Its Modeling of Cultivated Black Soil Slopes Affected by Thawed Depth*; China Agricultural University: Beijing, China, 2018. (In Chinese)
18. Li, Z.; Lu, K.; Ding, W. Experimental study on dynamic processes of soil erosion on loess slope. *J. Soil Water Conserv.* **2002**, *16*, 5–7+49. (In Chinese) [CrossRef]
19. Ban, Y.; Lei, T. Impact of frozen layer and rock fragment on sediment transport capacity on frozen-stony slopes. *Hydrol. Process.* **2022**, *36*, e14627. [CrossRef]
20. Wu, Y.; Ouyang, W.; Hao, Z.; Yang, B.; Wang, L. Snowmelt water drives higher soil erosion than rainfall water in a mid–high latitude upland watershed. *J. Hydrol.* **2018**, *556*, 438–448. [CrossRef]
21. Zhang, L.; Ren, F.; Li, H.; Cheng, D.; Sun, B. The influence mechanism of freeze–thaw on soil erosion: A Review. *Water* **2021**, *13*, 1010. [CrossRef]
22. Larsen, K.; Jonasson, S.; Michelsen, A. Repeated freeze-thaw cycles and their effects on biological processes in two arctic ecosystem types. *Appl. Soil Ecol.* **2002**, *21*, 187–195. [CrossRef]

23. Iwata, Y.; Yanai, Y.; Yazaki, T.; Hirota, T. Effects of a snow-compaction treatment on soil freezing, snowmelt runoff, and soil nitrate movement: A field-scale paired-plot experiment. *J. Hydrol.* **2018**, *567*, 280–289. [CrossRef]

24. Chen, C.; Lei, T.; Ban, Y. Influence of slope, flow rate, and thawed depth on soil detachment rate in partially thawed black soils. *J. Hydrol.* **2021**, *603*, 127009. [CrossRef]

25. Ban, Y.; Lei, T.; Liu, Z.; Chen, C. Comparison of rill flow velocity over frozen and thawed slopes with electrolyte tracer method. *J. Hydrol.* **2016**, *534*, 630–637. [CrossRef]

26. Wang, L.; Zheng, F.; Zhao, L.; Mo, S.; Qin, Q.; Geng, H.; Zhao, Y. Impacts of seepage flow and soil thaw depth on hill slope snowmelt erosion in Chinese Mollisol region. *J. Appl. Ecol.* **2021**, *32*, 4177–4185.

27. Li, G.; Zheng, F.; Lu, J.; An, J. The influence of rainfall and terrain factors on soil erosion process on black soil slopes. *Agric. Mach. J. Mech. Eng.* **2015**, *46*, 147–154. (In Chinese)

28. An, J.; Zheng, F.; Lu, J.; Li, G. Investigating the role of raindrop impact on hydrodynamic mechanism of soil erosion under simulated rainfall conditions. *Soil Sci.* **2012**, *177*, 517–526. [CrossRef]

29. Ding, B.; Zhang, J.; Zheng, P.; Li, Z.; Wang, Y.; Jia, G.; Yu, X. Water security assessment for effective water resource management based on multi-temporal blue and green water footprints. *J. Hydrol.* **2024**, *632*, 130761. [CrossRef]

30. Yang, H.; Wei, C.; Sun, G.; Tao, X.; Wang, Y. Responses of soil and ammonia nitrogen loss rates to hydraulic parameters under different slope gradients and rainfall intensities. *Water* **2024**, *16*, 230. [CrossRef]

31. Wang, L.; Zheng, F.; Zhang, X.; Wilson, G.V.; Qin, C.; He, C.; Zhang, J. Discrimination of soil losses between ridge and furrow in longitudinal ridge–tillage under simulated upslope inflow and rainfall. *Soil Till. Res.* **2020**, *198*, 104541. [CrossRef]

32. Li, G.; Zheng, F.; Lu, J.; Xu, X.; Hu, W.; Han, Y. Inflow rate impact on hillslope erosion processes and flow hydrodynamics. *Soil Sci. Soc. Am. J.* **2016**, *80*, 711–719. [CrossRef]

33. Zhang, P.; Yao, W.; Xiao, P.; Liu, G.; Yang, C. Study on the interaction and superposition effect of multi–dynamic erosion in the soft sandstone area of the Yellow River basin. *J. Hydrol.* **2022**, *53*, 109–116. [CrossRef]

34. Tian, P.; Xu, X.; Pan, C.; Hsu, K.; Yang, T. Impacts of rainfall and inflow on rill formation and erosion processes on steep hillslopes. *J. Hydrol.* **2017**, *548*, 24–39. [CrossRef]